Supporting Information

# Ferroelectric polymer nanopillars arrays on flexible substrate by reverse nanoimprint lithography

Jingfeng Song,[1] Haidong Lu,[1] Keith Foreman[1], Shumin Li,[2] Li Tan,[2] Shireen Adenwalla,[1]Alexei Gruverman[1] and Stephen Ducharme[1]

[1]Department of Physics and Astronomy & Nebraska Center for Materials and Nanoscience, University of Nebraska, Lincoln, NE 68588-0299, USA

[2]Department of Mechanical and Materials Engineering & Nebraska Center for Materials and Nanoscience, University of Nebraska, Lincoln, NE 68588-0526, USA

### Pressure measurement

We used the Omega Universal Load Cell to measure the pressure applied onto our sample during the reverse nanoimprint lithography process through the SPECAC hydraulic press system. Since the imprinting temperature of 135 °C is beyond the working temperature of the Load Cell, we recorded the pressure-time curve at 25 °C, which is shown in Fig. S**1**. The initial pressure of 3 bar slowly decreased to 2.6 bar after 60 minutes, and to 2.2 bar after another 90 minutes when the pressure was manually released. The exactly same starting pressure of 3 bar was used when doing our reverse nanoimprint lithography experiment at 135 °C, the pressure value could be slightly different from 2.6 bar over 60 minutes. The reason for the pressure decrease may be due to the relaxation of the sample and limitation of the design of the hydraulic press system to hold a small pressure for extended period of time.

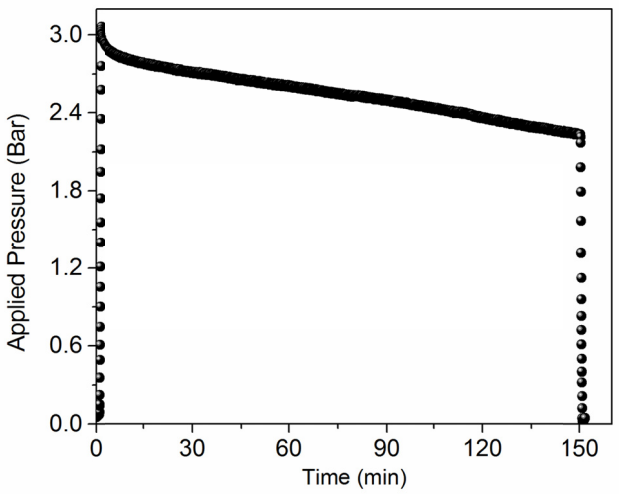


**Figure S1**. The pressure applied onto the sample during the reverse nanoimprint lithography process with respect to time measured at 25 °C.

### Nanopillar array with hexagonal arrangement

The soft mold based low-pressure reverse nanoimprint lithography is also highly customizable based on the initial silicon nanostamps chosen. By choosing a hexagonal arranged silicon nanostamp to prepare our PDMS soft molds, we were also able to fabricate large area, uniform P(VDF-TrFE) nanopillars on a PET substrate with hexagonal arrangements as is shown in Fig. S2. The copolymer nanopillars are 99 ± 3 nm in height, 676 ± 8 nm in period, and an average of 250 ± 6 nm from the top and bottom widths as measured from the AFM 3D topography and line scan in Fig. S2. The sizes and periodicity of the nanopillars were very close to the copolymer nanopillars in the rectangular arrangement shown in Fig. 2a.

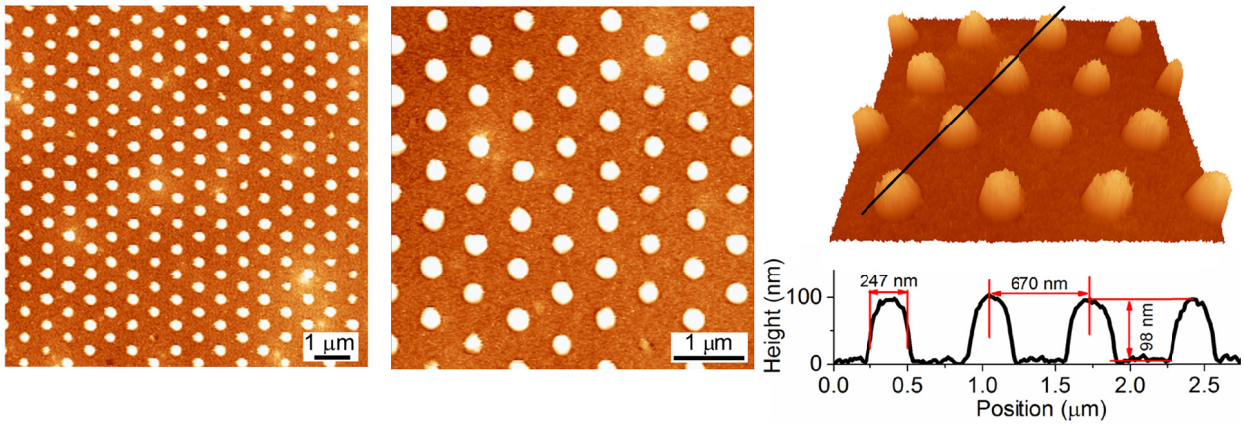


**Figure S2.** AFM topography of the P(VDF-TrFE) nanopillars with hexagonal arrangements and the line scan profile along the black line indicated on the 3D topography image.

### Langmuir-Blodgett deposition of terpolymer capping layer

The terpolymer of vinylidene fluoride (55.8%), trifluoroethylene (35%), and chlorofluoroethylene (9.2%) or P(VDF-TrFE-CFE), from Kunshan Hisense Electronics Co., Ltd., was used as received and dissolved in dimethylsulfoxide to a concentration of 0.05% by weight. The thin film of 45 nominal monolayers was transferred to the sample surface by horizontal Langmuir-Blodgett (LB) deposition at a surface pressure of 10 mN/m. The method of sample preparation and the properties of produced films are described in greater detail elsewhere.[1]

### Calculation of effective coercive voltage of nanopillars

Since polarization reversal occurs at the coercive field[2] and the polarization reversed when the phase value was close to 90°. In order to calculate the effective coercive voltage of the copolymer nanopillars in the multilayer capacitors, we first acquired the polarization reversal voltages of –15.4 ± 0.25 V and 26.5 ± 0.3 V, respectively, by inspecting the x-intercepts of the

phase diagram with a horizontal line at 90° phase (dashed line in Fig. 5b). From the half-width of the phase loop, we calculated the coercive voltage of the nanopillar capacitor $V_c$ to be 21.0 ± 0.3 V. The approximate 5 V shift of the coercive voltage to the negative voltage direction and asymmetric curves could be due to the difference of the work function of electrodes and asymmetric electric contact of the ferroelectric polymer with the top and bottom electrodes.[3, 4] The 45 ML terpolymer insulation layer was the main cause of the coercive voltage increase, as shown below. The AFM topography of the terpolymer coated nanopillars with hexagonal arrangement is shown in Fig. S3a, with the corresponding line scans of the nanopillars and terpolymer coating illustrated in Fig. S3b. The copolymer nanopillar, terpolymer coating and aluminum top electrode is indicated with green, yellow and gray color respectively in Fig. S3b. The finite element modeling (FEM) results of the applied voltage distribution over the nanopillars using Maxwell software are shown in Fig. S3c. The thickness of the 45 ML terpolymer layer is 180 nm with 4 nm per monolayer.[5] The thickness of the copolymer nanopillar layer is 90 nm according to previous AFM measurements. The dielectric constant of the copolymer is 10,[6] and the dielectric constant of terpolymer is 50.[7, 8] The much higher dielectric constant of the terpolymer is beneficial for obtaining a higher voltage drop across the ferroelectric copolymer layer. The applied voltage distribution across the center of a pillar (indicated with a white dashed line in Fig. S3c) is illustrated in Fig. S3d. The voltage drop across the copolymer nanopillar according to the modeling calculation is 24 V, which is 60% of the applied 40 V voltage. Based on the proportionality of the voltage drop across the nanopillar and the applied voltage in modeling result, the effective coercive voltage of the copolymer nanopillar $V_c(\text{eff}) = Vc \times 60\%$ was 12.6 ± 0.2 V.

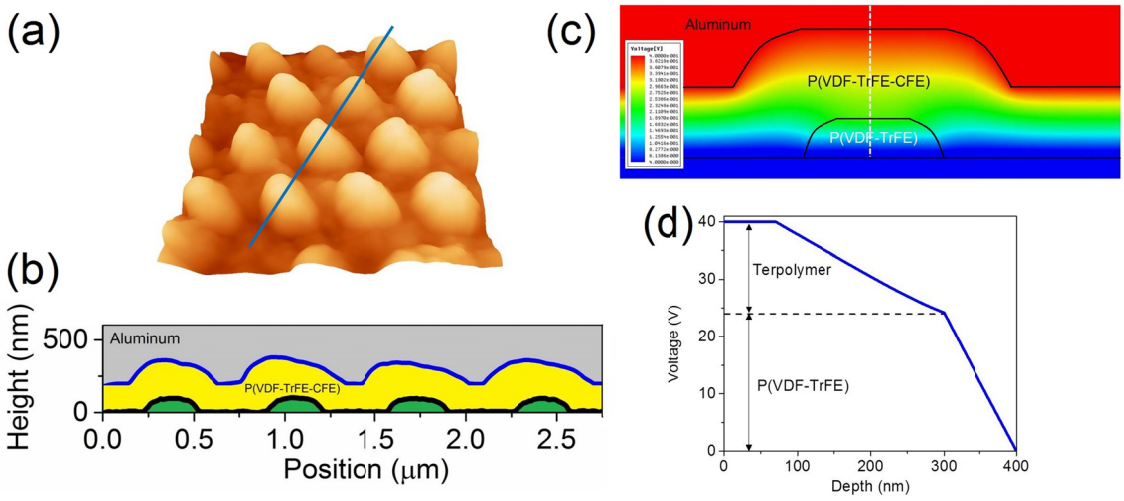


**Figure S3**. (a) AFM topography of the terpolymer coated P(VDF-TrFE) nanopillars. (b) Comparison of the AFM line scan result of nanopillar (black curve) and terpolymer coated nanopillar (blue curve). (c) Voltage drop distribution over the aluminum/terpolymer/nanopillar multilayer region with FEM method. (d) Voltage drop along the white dashed line in (c).

## References


1. S. Poddar and S. Ducharme, *Appl Phys Lett*, 2013, **103**, 202901.
2. M. E. Lines and A. M. Glass, *Principles and applications of ferroelectrics and related materials*, Clarendon Press, Oxford Eng., 1977.
3. S. J. Kang, I. Bae, Y. J. Shin, Y. J. Park, J. Huh, S. M. Park, H. C. Kim and C. Park, *Nano Lett*, 2011, **11**, 138-144.
4. F. Xia and Q. M. Zhang, *Appl Phys Lett*, 2004, **85**, 1719-1721.
5. S. Poddar, K. Foreman, S. Adenwalla and S. Ducharme, *Appl Phys Lett*, 2016, **108**, 012908.
6. S. Ducharme, S. P. Palto and V. M. Fridkin, in *Ferroelectric and Dielectric Thin Films*, ed. H. S. Nalwa, Academic Press, San Diego, 2002, vol. 3, pp. 545-591.
7. B. J. Chu, X. Zhou, B. Neese, Q. M. Zhang and F. Bauer, *IEEE T Dielect El In*, 2006, **13**, 1162-1169.
8. J. L. Wang, X. J. Meng, S. Z. Yuan, J. Yang, J. L. Sun, H. S. Xu and J. H. Chu, *Appl Phys Lett*, 2008, **93**.